IOSR Journal of Applied Physics (IOSR-JAP)
e-ISSN: 2278-4861.Volume 7, Issue 6 Ver. II (Nov. - Dec. 2015), PP 71-77
www.iosrjournals

Analysis of Phase Error and Cross Talk for the Young Interferometer Immunosensor

Moisi Xhoxhi[1], Joan Jani[2], Partizan Malkaj[3]
[1,2,3]*Department of Engineering Physics, Faculty of Engineering Mathematics and Engineering Physics, Polytechnic University of Tirana, Street "Muhamet Gjollesha", Tirana, Albania*

Abstract: *An analysis of the factors that influence the measurement errors of the four channel Young interferometer (YI) immunosensor are discussed and some possible techniques to reduce them are tested. Through the use of Matlab software, the effect of CCD camera resolution, Hanning window, and noise averaging on phase error (PE) and cross-talk (CT) is tested. It is shown that the increase of CCD camera resolution up to 2048 pixels reduces significantly PE and CT. Applying the Hanning window on the final interference pattern resulted effective in reducing the spectral leakage from the Fourier-transformed signal. With this method a reduction of PE and CT with an approximate factor of 5.2 was realized. The noise averaging method from signal overlapping was associated with the rapid reduction of PE and CT for up to 16 signals with an approximate factor of 7.58. A further increase in the number of overlaps impacted very little on PE and CT reduction.*

I. Introduction

The recent years have seen an increasing use of integrated optical sensors on the scientific research field and biomedical analysis since they can be used for the direct detection of biomolecular interactions. Thanks to the tremendous advances in microelectronics, nowadays it is possible the mass production of microsystems by hybrid integration of sources, sensors, photodetectors and CMOS electronics. These factors allow the fabrication of these sensors with a low cost and optimized characteristics such as high sensitivity, mechanical stability and possibility of miniaturization [1]. Many techniques exist in optical sensing but interferometry is one of the most sensitive ones [2]. It can measure small changes that occur in an optical beam along its propagation path due to the changes in the length of the beam's path, change in the wavelength of the beam, change in the refractive index of the media where it propagates, or any combination of these. Biosensing systems based on interferometry commonly measure the change in the effective refractive index of the medium Δn_{eff}, which is translated in the phase change of the propagating wave [3]. They can be easily integrated in an optical system and their characteristics can be used to measure different parameters by analyzing the interference of beams arising from the optical system. These are called interferometric biosensors which give the possibility to measure simultaneously several binding processes by the use of specific receptors in the measuring channels.

The origins of optical interference and interferometry date back to the experiments conducted by Thomas Young in 1803 [4]. Since his experiments, many interferometers that find application in chemical or biochemical measurements, such as Michelson, Fabry-Perot, Mach-Zehnder and Young, have been developed [5]. While the Michelson and Fabry-Perot interferometers need prior reference measurements and introduce additional complexity with their moving mirrors, the Mach-Zehnder and Young interferometers have no moving parts and have built in self-referencing, so that real-time monitoring is possible. For these reasons the latter interferometers have found a wider usage in chemical and biochemical measurements. Mach-Zehnder directs the beams to converge in a single channel, whereas the Young interferometer uses the natural beam divergence to interfere with each other. It generates a complete periodic intensity pattern that allows to determine the absolute sign of the induced phase change and produces a linear correlation between the spatial change of the interference pattern and the induced phase change [6]. By continuously recording the interferogram, real-time monitoring of biological events can be enabled.

This paper analysis the factors that influence the measurement errors of the four channel Young Interferometer (YI) immunosensor [7] and discusses some possible techniques to be applied in order to reduce them. By simulating this device in Matlab software the effect of Hanning window, CCD camera resolution and noise averaging in the reduction of measurement errors will be analyzed.

II. Integrated optical YI working principle

This paragraph will give a theoretical description of YI working principle The principle of a YI with four integrated optical channels, presented by Ymeti in 2004 [7], is similar to that with two channels presented by Brandenburg et al., in 2000 [8]. All channel pairs from the four channel integrated YI act as a two-channel

YI, each with a unique distance between them. The laser light splits into four parallel channels by using three Y-junctions, as shown in figure 1. The divergent output beams from these channels are in phase since they travel an equal optical path. Due to their overlapping they produce an interference pattern which is recorded by a CCD camera at a particular distance. Each channel pair in the multichannel YI device has a unique interdistance. There are six different channel pairs and the distances between them are d_{12} = 60 μm, d_{23} = 80 μm, d_{34} = 100 μm, d_{13} = 140 μm, d_{24} = 180 μm, and d_{14} = 240 μm. The optical path length difference of the beams originating from the four sources varies along the *y* axis of the CCD camera, which is chosen to be parallel to the axis defined by the four sources. The intensity distribution of the total interference pattern along the *y* axis on the CCD camera can be written as [9]:

$$I(y) \approx \sum_{i=1}^{4} I_i + 2 \sum_{i,j=1;i<j}^{4} (I_i I_j)^{\frac{1}{2}} cos\left(\Delta\Phi_{ij}(y) - \Delta\phi_{ij}\right) \quad (1)$$

where I_i and I_j are the output power from channels *i* and *j*, respectively. $\Delta\Phi_{ij}(y)$ is the phase difference between the interfering beams coupled out from channels *i* and *j* as a result of their different optical path length at the interfering position on the CCD camera. The phase change $\Delta\phi_{ij}$ represents the sum of the initial phase difference at the channel outputs in absence of the measurand, $\Delta\phi_{ij}^{0}$, and the phase change $\Delta\varphi_{ij} = \Delta\varphi_i - \Delta\varphi_j$ induced by refractive index changes Δn_i and Δn_j in channels *i* and *j*, respectively. The individual interference pattern produced from a certain channel pair, *i* and *j*, on the CCD camera, has a spatial frequency of the fringes calculated by:

$$k_{ij} = \frac{1}{\lambda}\frac{d_{ij}}{L} \quad (2)$$

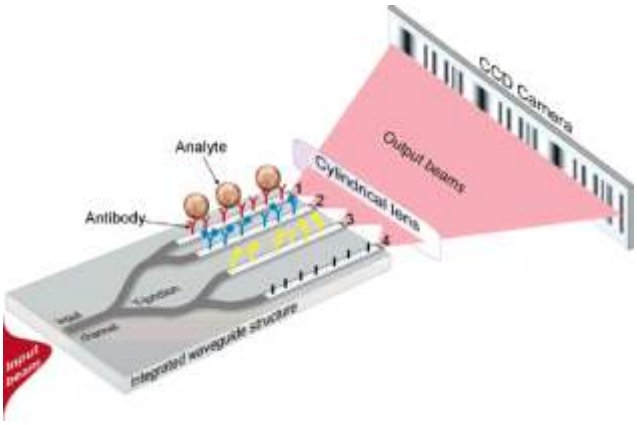

Figure 1 Schematic representation of the four-channel integrated optical YI biosensor: 1, 2 and 3 indicate the measuring channels, and 4 is the reference channel. Adapted from "Fast, ultrasensitive virus detection using a Young Interferometer sensor" by A. Ymeti et al., 2007, Nano Letters, 7, p. 394-397. Copyright 2007 by the American Chemical Society.

where d_{ij} is the distance between the channels *i* and *j*, and *L* is the distance from the channel endface to the CCD camera. The spatial frequency k_{ij} gives the number of fringes per unit length for the individual interference pattern. The refractive index changes in channels *i* and *j* can be induced due to binding between analyte and receptor molecules in the sensing window of each channel. The resulting refractive index change can cause a spatial shift of Δy_{ij} of the individual interference pattern which can be measured from the CCD camera. One can measure the change in refractive index between channels *i* and *j* from the following equation:

$$\Delta n_{ij} = \frac{d_{ij}}{lL}\left(\frac{\partial N_{eff}}{\partial n}\right)\Delta y_{ij} \quad (3)$$

If one chooses channel *i*, *i* = 1, 2, 3 as measuring channels and channel 4 as the reference one, the refractive index changes Δn_{14}, Δn_{24} and Δn_{34} can be calculated from the spatial shifts Δy_{14}, Δy_{24}, and Δy_{34} using equation (3) [10].

Calculating the Fast Fourier Transform (FFT) of the total interference pattern will result in six different peaks in the amplitude of the transformed signal. Having different distances d_{ij} for each channel pair, different spatial frequencies k_{ij} will be produced for the individual interference patterns. This makes it possible to separate the different peaks in the amplitude of the Fourier-transformed signal and select the spatial frequency for each peak. As a result, the phase change $\Delta\phi_{ij}$ between both channels of one pair, corresponding to the selected

spatial frequency k_{ij}, can be monitored independently from the other channel pairs. If a phase change is introduced in one of the channels, e.g. in channel 1, the same phase change is expected between channel pairs that involve channel 1. In the phase part of the FFT transformed signal one can see the phase change corresponding to channel pairs where channel 1 is involved. In this way, it is possible to monitor independently and simultaneously three different binding events from the three different measuring channels.

III. Analysis of phase error and cross-talk

From the calculations done with the real four channel YI device, when a phase change is introduced in one of the channels, there is a deviation between the resulting phase changes in the channel pairs and the expected ones [10]. The deviation from the expected phase changes is noted as phase error (PE), whereas the deviation where no phase change is expected is noted as cross-talk (CT). Concretely, it is observed that if a phase change of $0.5 \times 2\pi$ is introduced in channel 1, the phase changes between channel pairs 1 and 2, 1 and 3, and 1 and 4 differ from the expected one with a maximum of $\sim 0.05 \times 2\pi$ [10]. In addition, a phase change is observed between channels 2 and 3, 3 and 4, and 2 and 4. It is also observed that PE and CT change periodically with a period of 2π and reach a maximum value when the phase change is $(N+0.5) \times 2\pi$, where N is an integer [11].

There are several factors that affect the appearance of such deviations. Among them we can mention:

- The existence of noise in the signal detected from the CCD camera
- The fact that FFT algorithm used for signal analysis, considers the signal periodic.
- The spatial frequencies of individual interference patterns do not match with the spatial frequencies determined from the CCD camera.
- Low resolution of the CCD camera, etc.

Some of the techniques that can be used to reduce PE and CT, which will be discussed in the following paragraphs, are:

- Increase the resolution of the CCD camera
- Application of windowing technique [12]
- Noise averaging through signal overlapping [13].

IV. Simulation results

4.1 PE and CT dependence from the CCD camera resolution

From the simulations done in Matlab software the PE and CT has been studied first for channel 1 by changing the phase of the signal in the range [0:2π] when using a CCD camera resolution of 512 pixels. The PE and CT dependence from the phase change is depicted in figure 2. The graphics show that PE and CT have a maximum value for a phase change around $0.5 \times 2\pi$, which is in accordance with the experiments done with the real device.

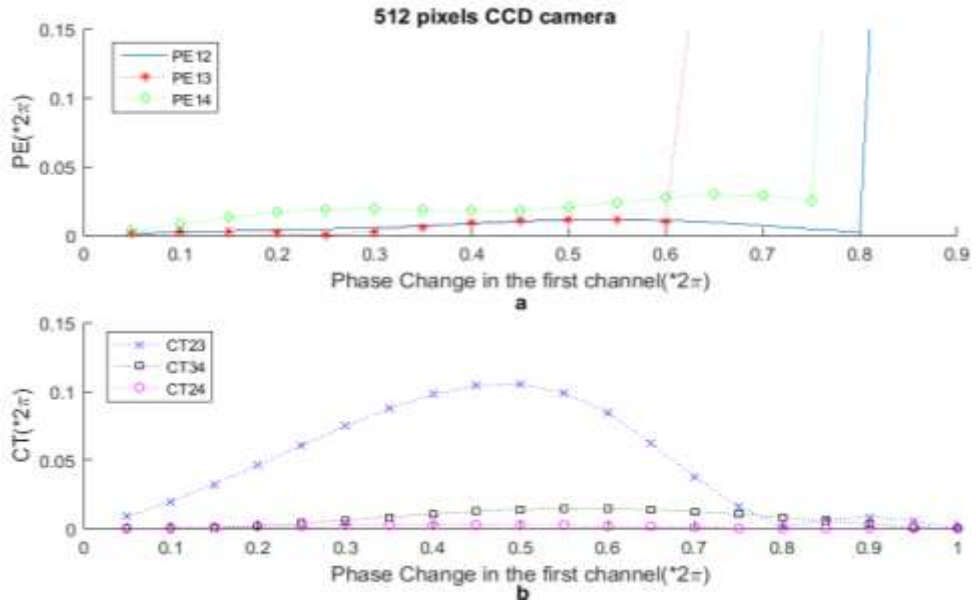

Figure 2 a) PE and b) CT dependence from the phase change in the first channel for a CCD camera resolution of 512 pixels

Figure 3 depicts the dependence of PE and CT for different values of the CCD camera resolution. The resolution values that we have been taken in consideration move in the range from 512 to 4096 pixels. These graphs show a significant reduction on PE and CT until the camera resolution reaches a value of 2048 pixels. A further increase on this value doesn't cause a significant reduction on PE and CT. These simulations are done for a constant phase change of $0.3*2\pi$ on channel 1. The reason why PE and CT reduces significantly with the increase of the CCD camera resolution is because the frequencies determined from FFT will be closer to the real spatial frequency of the interference pattern when the signal is sampled with denser points. As a consequence, the spectral leakage which arises from FFT will be reduced, leading to the reduction of PE and CT.

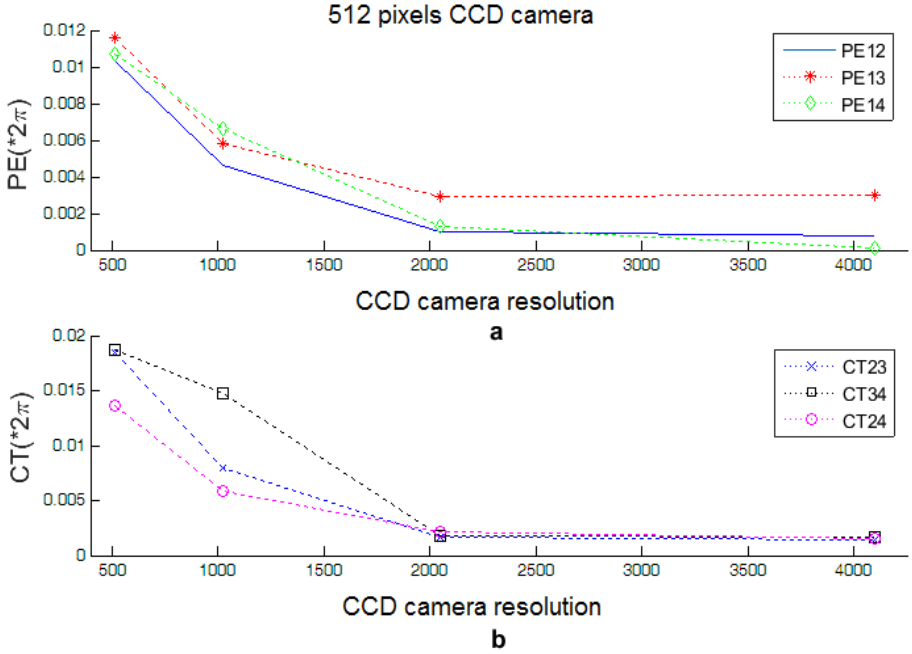

Figure 3 a) PE and b) CT dependence from the CCD camera resolution

4.2 PE and CT dependence from the Hanning window

Different window functions in the time domain can be used to reduce the spectral leakage caused by the implementation of FFT on a signal that does not contain an integer number of periods [14]. Since the signal is considered periodic from FFT, the multiplication of a finite signal with a window function makes the endpoints of the signal to match when applying the FFT. As a result, there will be a continuous signal and this will reduce the spectral leakage resulting in a more accurate calculation of the frequency spectrum of the signal through FFT. There exist different window functions each of which has its own frequency spectrum. Some of the most important window functions are Blackman-Harris, Kaiser-Bessel, Hanning and rectangular window [15]. In our simulations we have taken in consideration the Hanning window. Figure 4 depicts the dependence of PE and CT from the phase change in channel 1 after applying the Hanning window on the final interference pattern. In the simulations we have considered again a CCD camera with 512 pixels. From the graph we note that there is a significant reduction in PE and CT with an approximate factor of 5.2 compared to the values when not applying the Hanning window. Therefore, the use of windowing technique will help to get more accurate measurements from YI immunosensor.

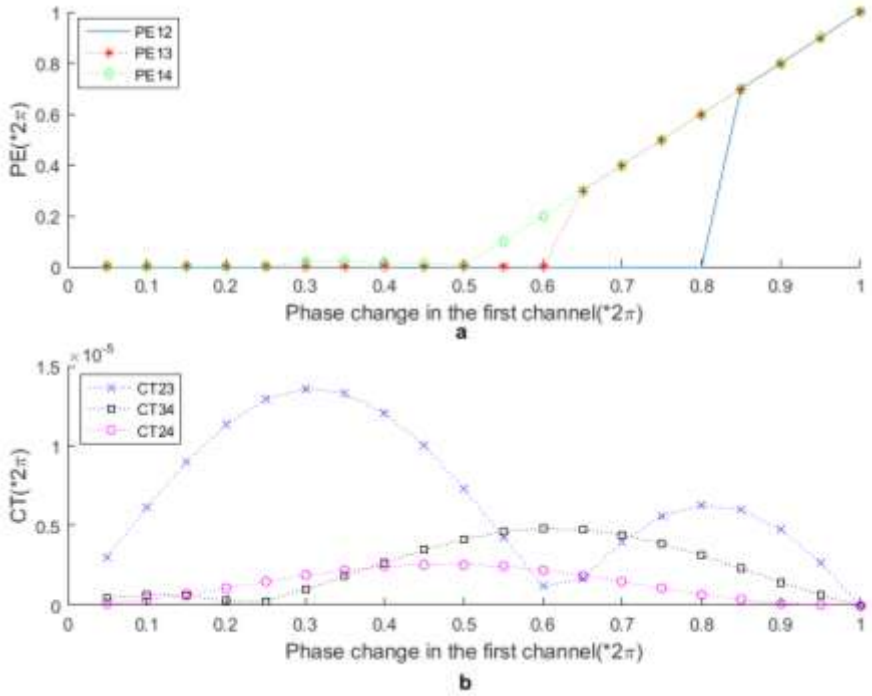

Figure 4 a) PE and b) CT dependence from the Hanning window

4.3 PE and CT dependence from signal overlapping

All the signals detected from a CCD camera contain some amount of noise which may come from the camera itself or from the outer environment. This noise is another factor that increases the values of PE and CT in YI immunosensor. A technique to reduce it consists in overlapping the signal of the same interference pattern taken from different records. Given that the noise has a random value in the signals that are overlapped, the noise final value will tend to a median, the growth rate of which will be smaller than the growth rate of the useful signal [13]. This will lead to a better signal-to-noise ratio in the final signal which will have lower values of PE and CT compared to the non-overlapped signal. This technique is known as noise averaging through signal overlapping. Figure 5 depicts the dependence of PE and CT from the number of overlapped signals when a phase change of 0.3*2π is introduced in channel 1. We have taken in consideration 4, 8, 16 and 32 overlapped signals, and in each case the inserted artificial noise signal is random. From the graphs we can observe that increasing the number of overlapped signals from 4 to 16 is associated with the reduction of PE and CT with an approximate value of 7.58. A further increase in the number of overlapped signals has a very small effect in the reduction of PE and CT. Therefore, we can conclude that using more than 16 overlapped signals

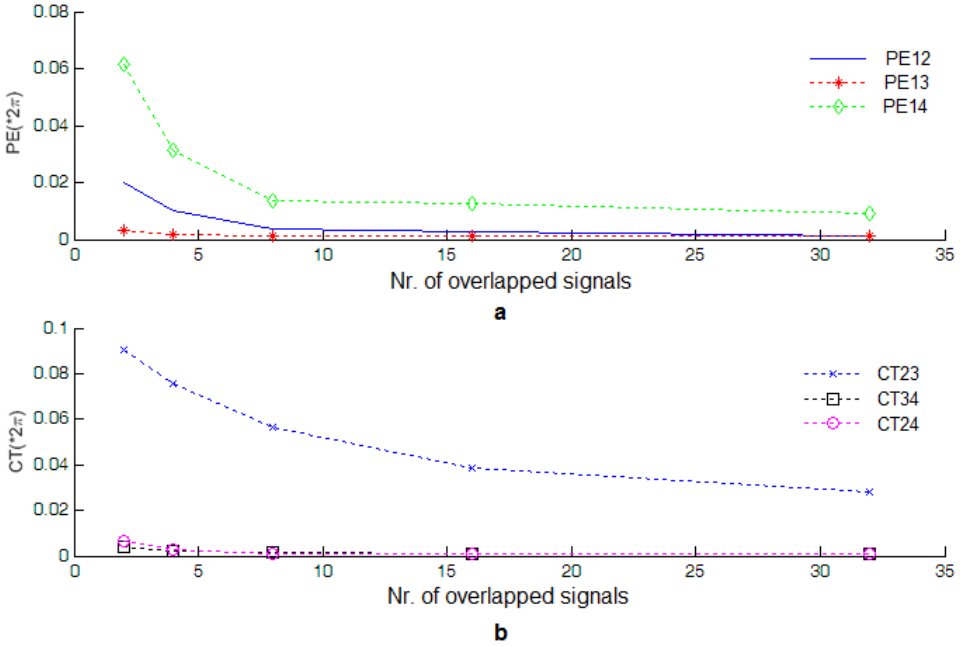

Figure 5 a) PE and b) CT dependence from the number of overlapped signals

would not give a significant improvement in the signal quality, besides increasing the processing time of the signal.

V. Conclusions

The results of measuring the concentration of analytes with the four channel integrated YI, the speed of implementation of a measurement and the very possibility of using this system to perform measurements on-site, depend directly on the sensitivity of the system to detect the phase changes in the individual interference patterns under the influence of very small concentrations of analytes in the sample. The most important factors that negatively affect this process are the own noise of the CCD cameras and the influence of signals from different channels. In our study we used three methods that tend to minimize the level of noise and spectral leakage. The simulations with different camera resolutions showed a significant reduction of PE and CT when the camera resolution increased up to 2048 pixels. A further increase on the camera resolution didn't reduce significantly further PE and CT. Applying the Hanning window on the final interference pattern resulted effective in reducing the spectral leakage from the Fourier-transformed signal. With this method a reduction of PE and CT with an approximate factor of 5.2 was realized. Lastly, the noise averaging method from signal overlapping was used to improve the signal to noise ratio in the final signal taken from the overlap of different numbers of the same signal. Increasing the number of overlapping signals was associated with the rapid reduction of PE and CT for up to 16 signals with an approximate factor of 7.58. A further increase in the number of overlaps impacted very little on PE and CT reduction.

References

[1]. Kooyman, R. and L. Lechuga, *Immunosensors based on total internal reflectance*. 1997, New York: CRC Press. p. 169-196.
[2]. Lukosz, W., *Principles and sensitivities of integrated optical and surface plasmon sensors for direct affinity sensing and immunosensing.* Biosensors and Bioelectronics, 1991. **6**(3): p. 215-225.
[3]. Schmitt, K., et al., *Evanescent field sensors based on tantalum pentoxide waveguides–a review.* Sensors, 2008. **8**(2): p. 711-738.
[4]. Young, T., *The Bakerian lecture: Experiments and calculations relative to physical optics.* Philosophical transactions of the Royal Society of London, 1804. **94**: p. 1-16.
[5]. Campbell, D.P., *Interferometric biosensors*, in *Principles of Bacterial Detection: Biosensors, Recognition Receptors and Microsystems.* 2008, Springer. p. 169-211.
[6]. Cross, G.H., Y. Ren, and N.J. Freeman, *Young's fringes from vertically integrated slab waveguides: applications to humidity sensing*. Journal of applied physics, 1999. **86**(11): p. 6483-6488.
[7]. Ymeti, A., *Development of a multichannel integrated Young interferometer immunosensor.* 2004.
[8]. Brandenburg, A., et al., *Interferometric sensor for detection of surface-bound bioreactions.* Applied Optics, 2000. **39**(34): p. 6396-6405.
[9]. Hecht, E., *Hecht optics.* Addison Wesley, 1998. **997**: p. 213-214.
[10]. Ymeti, A., et al., *Realization of a multichannel integrated Young interferometer chemical sensor.* Applied optics, 2003. **42**(28): p. 5649-5660.
[11]. Ymeti, A., et al., *Fast, ultrasensitive virus detection using a Young interferometer sensor.* Nano Letters, 2007. **7**(2): p. 394-397.
[12]. Harris, F.J., *On the use of windows for harmonic analysis with the discrete Fourier transform.* Proceedings of the IEEE, 1978. **66**(1): p. 51-83.

[13]. Potzick, J., *Noise averaging and measurement resolution (or "A little noise is a good thing").* Review of scientific instruments, 1999. **70**(4): p. 2038-2040.
[14]. Kay, S.M. and S.L. Marple Jr, *Spectrum analysis—a modern perspective.* Proceedings of the IEEE, 1981. **69**(11): p. 1380-1419.
[15]. Heinzel, G., A. Rüdiger, and R. Schilling, *Spectrum and spectral density estimation by the Discrete Fourier transform (DFT), including a comprehensive list of window functions and some new at-top windows.* 2002.